Energy Advances

ROYAL SOCIETY OF CHEMISTRY

PAPER

View Article Online
View Journal | View Issue

Cite this: *Energy Adv.*, 2023, **2**, 1674

A 3D-hierarchical flower like architecture of anion induced layered double hydroxides for competing anodic reactions†

Krishankant, Aashi, Baljeet Kaur, Jatin Sharma, Chandan Bera and Vivek Bagchi *

Received 1st May 2023,
Accepted 16th August 2023

DOI: 10.1039/d3ya00188a

rsc.li/energy-advances

The ongoing challenge in producing clean energy is to find highly active non-noble metal-based electrocatalysts. To overcome the high theoretical potential of the oxygen evolution reaction (OER, 1.23 V), alternative anodic reactions such as the urea oxidation reaction (UOR) may be considered to boost hydrogen generation. In this study, sulfur was incorporated into CoFeLDH to synthesize a S-CoFeLDH catalyst through the process of sulfurization, using Na_2S as the sulfur source. The catalyst showed an overpotential of 171 mV for the UOR and 268 mV for the OER, at a current density of 40 mA cm^{-2}. The catalyst also exhibited superior stability, with more than 100 hours of performance for both the OER and UOR at higher current densities. A full cell was constructed using a S-CoFeLDH||Pt/C electrode, which requires a potential of 1.52 V and 1.41 V for overall water and urea electrolysis, respectively. Density functional theory (DFT) was used to analyse the catalyst's activity and active sites by calculating its Gibbs free energy. The DFT results indicate that "Co" is the more prominent active site for the OER in S-CoFeLDH and the density of states (DOS) calculation predicts a favourable UOR.

Introduction

Human activity is the primary cause of climate change, which is a reality. The amount of greenhouse gases present in the earth's atmosphere has a direct impact on the planet's average global temperature. Since the Industrial Revolution, the average world temperature has been gradually increasing. Carbon dioxide (CO_2), the most prevalent greenhouse gas and the one that makes up nearly two thirds of all greenhouse gases, is the major byproduct of the combustion of fossil fuels,[1] which led to an unprecedented climate change that is accompanied by a significant loss of life in many regions of the world. Switching to clean sources of energy is the only option we have to save this planet. Geothermal, wind, water, and tidal energies are the most potential renewable sources which can be used for carbon neutral energy conversion. Utilization of green energy for the electrochemical water splitting can be one of the best energy producing approaches we can think of. However, the slow kinetics involved in the oxygen evolution reaction (OER) restricts the efficiency of hydrogen evolution as well. The production of an efficient and stable electrocatalyst is pivotal in solving the problem of slow anodic reaction kinetics. In the OER, the large overpotential (1.23 V) results in a large energy consumption, which limits the large-scale production of hydrogen.[2] Thus, investigating other alternative anodic reactions, for example, ethanol, methanol, hydrazine and urea is also an option for energy-conversion.[3–6] To overcome the high theoretical potential of 1.23 V of the OER, the UOR can be performed which requires only 0.37 V for the oxidation process.[7,8] Thus, the OER and UOR are considered as the competing anodic reactions for energy production, and thus it is desired to develop a catalyst which can perform better for efficient hydrogen production. Increasing industrialization has significantly escalated the environmental problems where more than 2 kilo-tons of urea are produced per day, while the amount of urea from human urine could be 120 times more than that.[9] The high concentration of urea in an aqueous system leads to the conversion of urea into ammonia, which further oxidizes into other pollutants like nitrites, nitrates and nitric oxides.[10] Direct disposal of urea-contaminated water has a detrimental effect on the environment.[11] Thus, an appropriate treatment of urea-rich waste-water is necessary. Therefore, it is very important to develop an efficient UOR catalyst, which can not only decontaminate the urea-rich waste water, but also helps in simultaneous H_2 production. The mechanism involved in the OER and UOR is:[12]

Institute of Nano Science and Technology, Sector-81, Knowledge City, Sahibzada Ajit Singh Nagar, Punjab, 140306, India. E-mail: vivekbagchi@gmail.com

† Electronic supplementary information (ESI) available: DFT details with formulae and data, catalyst comparison, and FESEM, XPS, LSV, impedance and CV results. See DOI: https://doi.org/10.1039/d3ya00188a

Overall water splitting reaction

$$2H_2O(l) \rightarrow 2H_2(g) + O_2(g)$$

$$\text{Anode} \rightarrow H_2O \rightarrow O_2 + 4H^+ + 4e^-$$

$$\text{Cathode} \rightarrow 2H^+ + 2e^- \rightarrow H_2(g)$$

$$\text{Overall UOR: } [CO(NH_2)_2] + H_2O + 6OH^- \rightarrow N_2 + 3H_2O + CO_2 + 6e^-$$

$$\text{Anode} \rightarrow CO(NH_2)_2 + 6OH^- \rightarrow N_2 + 5H_2O + CO_2 + 6e^-$$

$$\text{Cathode} \rightarrow 6H_2O + 6e^- \rightarrow 3H_2 + 6OH^-$$

Layered double hydroxides (LDHs) have emerged as a promising and reliable electrocatalyst for the OER.[13] A four-step process of oxygen evolution is carried out by H^+ transfer, which plays a crucial role in the oxidation of water and the formation of metal hydroxides or oxyhydroxides.[14] Negatively charged intermediates (O^-, OH^- and OOH^-) which are formed during the OER can be easily incorporated into the positively charged LDH sheets.[15] However, LDH materials are not well explored for the UOR. Doping a heteroatom into the LDH system can significantly increase the electrochemical activity of the catalyst. Recently in 2022, Patil *et al.* have reported an article on "Engineered 2D Ni hydroxide nanosheets with fluorine for highly active electrocatalyst for OER and UOR".[16] F–Ni$(OH)_2$ exhibits excellent OER and UOR activity with onset potentials of 1.43 and 1.16 V *vs.* RHE, at 10 mA cm^{-2}, respectively. Heteroatom doping allows for the development of efficient, non-noble-metal-based electrocatalysts for water and urea electrolysis using a simple and scalable method. Sulfur has many physicochemical properties, and turns out to be fascinating when doped into existing electro-catalysts. Doping a conventional catalyst with sulfur presents a new perspective to revitalize the established technology by modifying the electronic properties of the material. Metal sulphides (MS) show different behaviors with different transition metals, for example, group IV–VII (Mo, W, Nb, *etc.*) MS adopt a solid structure of graphite like layered orientation and group VIII–XII (Co, Fe, Ni, *etc.*) MS form a non-layered structure.[17] Non-layered metal sulphides, M_xS_y, generally form a pyrite and marcasite structure with $x = 1$ and $y = 2$.[18] Subbaraman *et al.* revealed that the enhanced electrochemical activity of metal-(oxy)hydroxide towards the OER is related to the weak bond strength of OH_{ads}–M^{n+}, which is accountable for the repulsion force between the d-band of metal ions and the bonded oxygen p-band centres.[19] Due to a repulsive interaction between the 3p and 2p orbitals of S and O, the electronegative S atom in LDH-MS prevents the coordination of –OH with Mn^+.[20] In the OER, the S element of MS can manifest more electrochemical active sites of LDHs. LDHs generally undergo self-reconstruction during the electrochemical reaction in an alkaline medium generating (oxy)hydroxides, which further act as active species for the OER. Considering the UOR, (oxy)hydroxides are also capable of catalysing the anodic reaction, in a more complexed $6e^-$ process.[21] Also the presence of conductive intermediates like nickel and copper foam plays a vital role in improving intrinsic charge transfer and optimizing the electrode stability.[22] Porous Ni foam behaves as a substrate to assist the 3D hierarchical framework growth on the surface during the *in situ* synthesis of a material on nickel foam.[23] Thus, substrates can also play a significant role in enhancing the electrochemical activity simply by changing the morphological platform. Using a conductive substrate for fabricating MS-LDHs may enhance the kinetics of the OER. The application of LDH-based materials in the UOR is not much explored as compared to the OER. Such an initiative can resolve twin problems of energy generation and waste treatment.

Herein, an innovative approach is developed to synthesize CoFeLDH nanostructures assimilated with sulphur on nickel foam. The detailed synthesis procedure is shown in Scheme 1. A 3D-hierarchical flower like architecture was made out of packed nanosheets of S-CoFeLDH, grown on nickel foam (NF). The S-CoFeLDH/NF catalyst showed an overpotential of 171 mV for the UOR and 268 mV for the OER, at a current density of 40 mA cm^{-2}. The catalyst also exhibited superior stability, with more than 100 hours of performance for both the OER and UOR at higher current densities. A full cell was

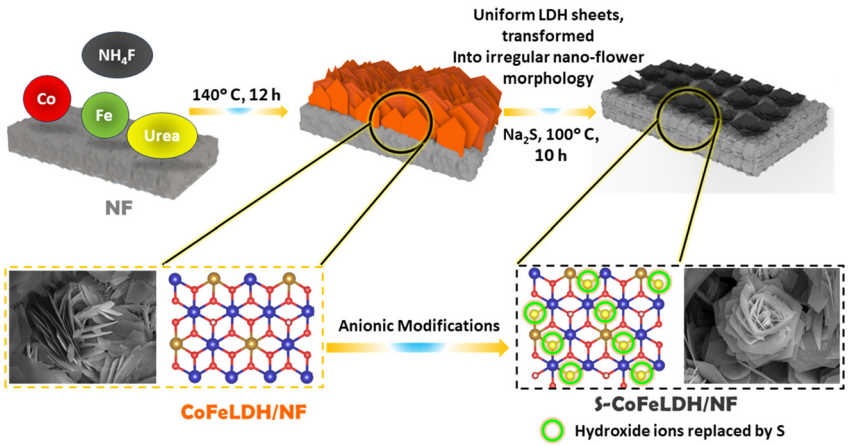

Scheme 1 The synthesis of S-CoFeLDH/NF and CoFeLDH/NF.

constructed using a S-CoFeLDH||Pt/C electrode, which requires a potential of 1.52 V and 1.41 V for overall water and urea electrolysis, respectively. The DFT study indicates Co as the most prominent active site in the catalytic process of the OER and the increased density of states (DOS) proves the increased orbital contribution which improves the electrocatalytic activity towards the OER and the UOR.

Experimental

Chemicals used

All the chemicals were used directly without any purification. Cobalt (Ous) nitrate hexahydrate ($Co(NO_3)_2$ $6H_2O$ purity > 98%), ferric nitrate nonahydrate (Fe $(NO_3)_3{\cdot}9H_2O$ with purity 98–101%), urea ($CO(NH_2)_2$ purity > 99.9%), ammonium fluoride (NH_4F ~99% purity), and potassium hydroxide (KOH 85% extra pure) were purchased from CDH chemicals Ltd. RuO_2 and NF were purchased from Aldrich corporation and Nano Shel India Ltd, respectively. All the solutions were prepared in deionized (D.I.) water.

Pre-treatment of Ni foam

Nickel foam (NF) of size 1 × 1 cm^2 was washed using an ultra-sonication method employing 1 M HCl as the washing reagent and then the washing was repeated using D.I water several times.

Synthesis of CoFeLDH/NF

The washed NF was used as a conductive substrate for material growth and placed in the reaction mixture in a Teflon lined stainless steel hydrothermal autoclave. The reaction mixture was prepared by adding 6 mmol Co(II) and 2 mmol Fe(III) into 40 mL D.I water. At the time of stirring 10 mmol urea was added to increase the basicity of the reaction mixture, followed by the addition of 5 mmol ammonium fluoride, which acts as a morphology-directing agent. The NF was placed in a slanting position in the autoclave and the resulting mixture was poured into it and kept in an oven at 140 °C for 12 h. It was then cooled down naturally. The resulting NF loaded with CoFeLDH was washed with deionized water to obtain brown coloured CoFeLDH uniformly grown over the NF. At 70 °C, CoFeLDH/NF was dried overnight in a vacuum oven.

Synthesis of S-CoFeLDH/NF

To synthesize S-CoFeLDH/NF, 0.62 g of $Na_2S.9H_2O$ was used as a sulphur source and dissolved in 40 mL of D.I water. The NF which contains CoFeLDH was immersed in the solution of $Na_2S{\cdot}9H_2O$ in a 50 mL hydrothermal autoclave and was placed in a hot air oven at 100 °C for 10 h. After the reaction is over, the solution was naturally cooled down and the NF was washed with deionized water. Finely coated black colored S-CoFeLDH/NF was formed on NF. After washing S-CoFeLDH/NF, the sample was dried at 70 °C overnight using a vacuum oven.

Structural characterization

X-Ray diffraction (XRD) analysis was performed on a Bruker-Eco D8-Advance diffractometer with Copper-kα radiation (λ = 1.54 Å) with a 2θ range of 10–70°. Elemental behaviour and binding energy were analysed using XPS (X-ray photoelectron spectroscopy) with Al kα monochromatic X-ray of 1486.7 eV photon energy. The morphological study was carried out using HRTEM and FESEM employing a JEM-2100 Plus with a 200 kV accelerating voltage and an Apereo 2 FESEM (Thermo Fischer), respectively. EDS (energy dispersive spectroscopy) was also used to analyse the uniform distribution of elements present in the sample using an Apereo 2 FESEM (Thermo Fischer).

Electrochemical details

All electrochemical experiments were conducted using a conventional three-electrode system and a Metrohm Multichannel Auto-lab. The system employed 1 M KOH for the OER and 1 M KOH + 0.5 M urea for the UOR. The three-electrode system consisted of an Ag/AgCl reference electrode in a 3 M KCl solution, a graphite rod as the counter electrode, and the synthesized catalyst as the working electrode. The working electrode was the NF coated with S-CoFeLDH. Linear sweep voltammetry (LSV) and cyclic voltammetry were performed at a low scan rate of 1 mV s^{-1} to avoid Ni^{2+} and Ni^{3+} electronic transitions.[24] EIS (electrochemical impedance spectroscopy) was performed over the frequency range of 0.01 Hz to 100 kHz at a particular applied potential. The chronoamperometric technique was used to analyse the stability of the catalyst. All electrochemical analyses were carried out at room temperature (25 °C). The potential is expressed in terms of the reversible hydrogen electrode (RHE) using the following formula:

$$E_{RHE} = E_{Ag/AgCl} + 0.198 + 0.0591 \times pH \quad (1)$$

Ruthenium oxide was used as the benchmark catalyst to compare the activity of the as synthesized material. To prepare a RuO_2 electrode, 2 mg of RuO_2 was dissolved in 495 μL of ethanol with 5 μL Nafion and the mixture was drop cast on the washed NF substrate. The electrochemically active surface area (ECSA) was determined by calculating C_{dl} in the non-faradaic region at different scan rates in 1 M KOH. To determine C_{dl}, a graph was constructed using the difference between $\Delta j(j_a - j_c)$ and the scanning rate as a variable. The ratio of C_{dl}/C_s is considered as the ECSA, whereas C_s is the specific capacitance of the material (NF) in 1 M KOH. The apparent turn over frequency (TOF) was also calculated to examine the activity and reusability of the catalyst, and the formula used for the same is:

$$TOF = Js/4mF \quad (2)$$

where J is the current density, s represents the size of the material activated in electrochemical analysis, m is the number of moles of the catalyst and F is the faradaic constant.

Computational details

Vienna *ab initio* simulation package (VASP) was used to perform the DFT calculations. The functionals used in the calculations are generalized gradient approximation (GGA) and Perdew–Burke–Ernzerhof (PBE) exchange functionals.[25] A super cell of $2 \times 2 \times 1$ was constructed with 15 Å vacuum allowed in the z-direction to restrict the periodic array interaction. Plane wave cut-off energy was set to be 520 eV with a $8 \times 8 \times 1$ λ-centred K-mesh. The convergence force was chosen as 0.001 eV $Å^{-1}$ and the energy convergence was set as 10^{-4} eV for structure relaxation. Gibbs energy relations were also discussed in the results and discussion section.

Results and discussion

Commercially available NF was used as a conductive substrate for the fabrication of a S-CoFeLDH/NF working electrode. The hydrothermal method was chosen to facilitate the sequential growth of S-CoFeLDH using the specified reagents outlined previously. The employed sulfurization involves an anion exchange process, which resulted in the replacement of several OH^- ions of CoFeLDH by the sulfide ions evolved from the Na_2S source.[26] The phases of the catalyst were analysed with XRD (Fig. 1(a)) where the characteristic peaks of CoFeLDH were observed. The peaks of the as synthesized material were observed at 2θ of 11.84°, 23.42°, 34.07°, 38.73°, 46.23°, 59.09° and 60.54° matching with the JCPDS card 00-050-0235 of CoFeLDH,[14] which belongs to the $R\bar{3}m$ space group with a rhombohedral unit cell, and the percentage of crystallinity was observed to be 61.7%. Also, the peaks at 45.6° and 52.5° were attributed to nickel foam (JCPDS 00-001-1266). In the S-CoFeLDH/NF PXRD patterns, it was found that after S incorporation (to CoFeLDH), there were peaks matching with those of CoFeLDH.[27] After the sulfurization process, the primary characterization peaks were retained in S-CoFeLDH/NF, however, the peak intensity decreases suggesting that the sulphur is responsible for weakening the crystallinity of S-CoFeLDH/NF, which reduces the percentage of crystallinity to 10.3%. The distribution of the electrons around the lattice is altered due to the S-doping. The resulting irregular arrangements of the atoms lead to reduced-crystallinity and produce structural defects. These structural changes create possible active sites, which enhance the mass and charge transfer of the catalyst.[28]

To further study the effect of sulfur incorporation into LDH, X-ray photoelectron spectroscopy (XPS) was performed. Elemental valence states and the chemical composition on the surface were revealed *via* XPS spectra. The wide scan spectra of S-CoFeLDH/NF and pristine CoFeLDH/NF are displayed in Fig. S1a (ESI†). It has been observed in the inset of ESI,† Fig. S1(a) that sulfur is present in the S-CoFeLDH spectrum, which indicates successful doping of the catalyst. In Fig. 1(b), the spectra of iron in CoFeLDH exhibit two peaks near 714.1 eV and 724.2 eV for Fe $2p_{3/2}$ and Fe $2p_{1/2}$, respectively,[29] indicative of the presence of Fe^{3+} ions.[30] After sulfurization, a shift in the Fe $2p_{3/2}$ binding energy peak was observed, suggesting the change in the electronic environment after the incorporation of S into the system. In Fig. 1(c), a high resolution spectrum of Co in CoFeLDH is shown, where two peaks were observed at 797.5 eV and 781.3 eV for Co $2p_{1/2}$ and Co $2p_{3/2}$, respectively,[31]

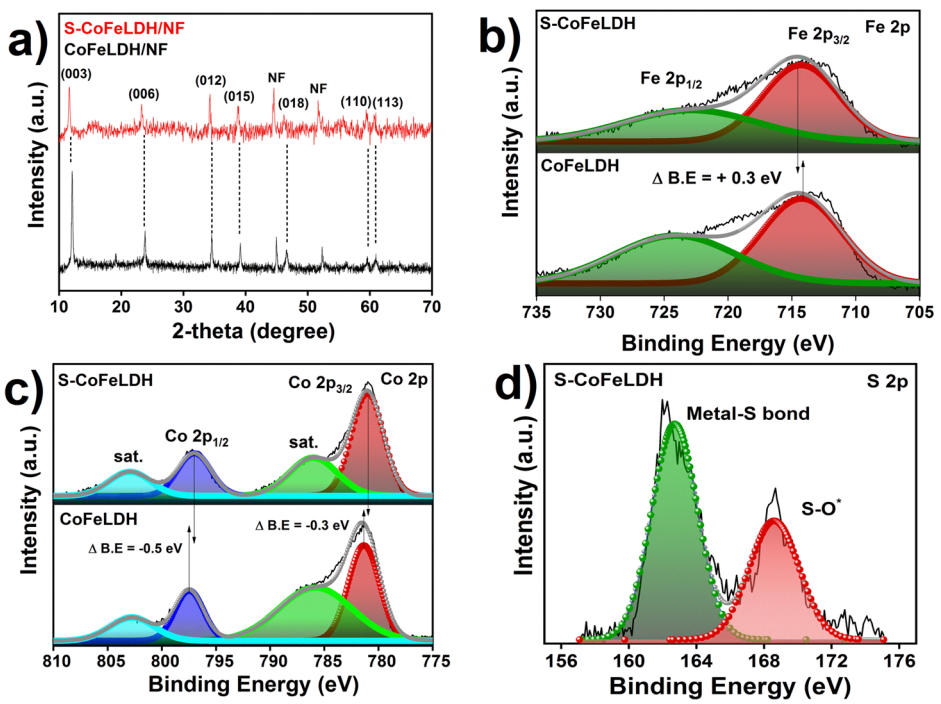

Fig. 1 (a) PXRD patterns of S-CoFeLDH/NF and CoFeLDH/NF. High resolution XPS of (b) Fe and (c) Co in S-CoFeLDH and CoFeLDH and (d) high resolution XPS of S corresponding to S-CoFeLDH.

confirming the presence of Co^{2+} in the catalyst.[32] Also the major satellite peaks were observed at about 785.6 eV and 802.7 eV for Co $2p_{3/2}$ and Co $2p_{1/2}$, respectively. After sulfur incorporation a negative shift was observed in the Co 2p XP spectra, indicating an alteration in the electronic environment. In Fig. 1(d), showing the S2p spectra, the peaks observed at 162.8 eV and 168.6 eV were attributed to the presence of a metal–sulphur bond, which makes sense, because some of the OH^- are being replaced with S^{2-} ions.[26] The peak observed at 168.6 eV is attributed to the S–O bond formed from the oxidized sulphate species.[33] All XPS patterns (Fig. 1(b)–(d)) suggest that the exterior of the catalyst is roofed with Co^{2+}, Fe^{3+}, S^{2-} and sulphate ions. In Fig. S1(b), ESI,† the O1s spectra show peaks attributed to the M–O and M–OH bonds, which are present in the catalyst. Specifically, the binding energy peaks of Co 2p and Fe 2p are shifted by −0.5 and +0.3 eV, respectively, after sulphur incorporation, suggesting the variation of the electronic environment of Co and Fe due to the incorporation of sulphur. As the polarization of S^{2-} is more effective as compared to oxygen anions, the replacement of hydroxyl anions by sulphur enhances the electron density over the catalytic surface, creating a reducing environment.[34–36]

The morphological details of S-CoFeLDH/NF and CoFeLDH/NF were revealed from FESEM and TEM micrographs as shown in Fig. 2. A 3D hierarchical flower like morphology of S-CoFeLDH/NF has been confirmed by FESEM in Fig. 2(a) and (b). Pristine CoFeLDH/NF sheets display fine and sharp features without any agglomeration (Fig. 2(c) and (d)). The micrographs and elemental maps of CoFeLDH are displayed in Fig. S2, ESI.† A homogeneous order of morphology was observed in FESEM images at different resolutions in Fig. 2(a) and (b). The micrographs of the catalyst reveal porous nanostructures made of nanosheets, which are distributed widely over the electrode. These structural aspects indicate a possibility to produce more electrochemical active sites and enhanced surface accessibility.[32] In Fig. 2(e), the TEM image of S-CoFeLDH/NF displays nanosheets with an average size of 250 nm. Also, in Fig. 2(f) the rough and porous nanosheets of S-CoFeLDH/NF show the clear lattice fringes of width 0.19 and 0.27 nm corresponding to the (018) and (012) planes, respectively. The inset of Fig. 2f shows the SAED pattern indicating the presence of major characteristic plane of LDH, (003). The HR-TEM phase studies reveal that the planes are in agreement with the XRD results (JCPDS 00-050-0235). In Fig. 2(g)–(k), STEM images show a uniform distribution of elements throughout the surface of the catalyst. In Fig. S3, ESI,† the EDX map of the catalyst displays and confirms the existence of all elements (Co, Fe, O and S) which suggests successful sulfurization of CoFeLDH.

The electrochemical activity of the catalyst was analysed in a 1 M KOH electrolyte with a slow scan rate of 1 mV s^{-1} using three electrode systems. For appropriate interpretation of the electrochemical activity of the catalyst, CoFeLDH/NF, RuO_2/NF and NF were included in the study for comparison. The oxidation peak located near 1.4 V shown in Fig. 3(a) corresponds to $Ni^{2+/3+}$ transitions. The LSV polarization curves of S-CoFeLDH/NF, CoFeLDH/NF, RuO_2/NF and NF exhibit an overpotential of 268, 364, 430 and 523 mV, respectively, to achieve a current density of 40 mA/cm.[2] To check the tendency of intrinsic activity of the catalyst, the OER kinetics was determined using

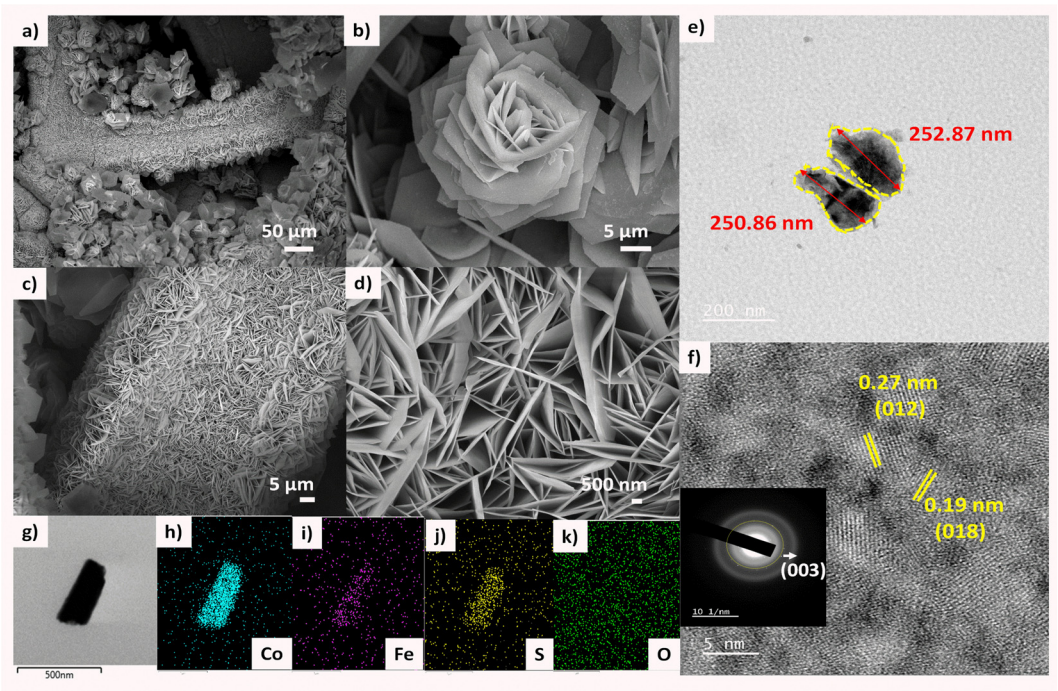

Fig. 2 FESEM images of (a) and (b) S-CoFeLDH/NF and (c) and (d) CoFeLDH at different resolutions. (e) TEM image, (f) HR-TEM image with the inset showing the SAED pattern of S-CoFeLDH/NF and (g)–(k) elemental maps of Co, Fe, S and O of S-CoFeLDH/NF.

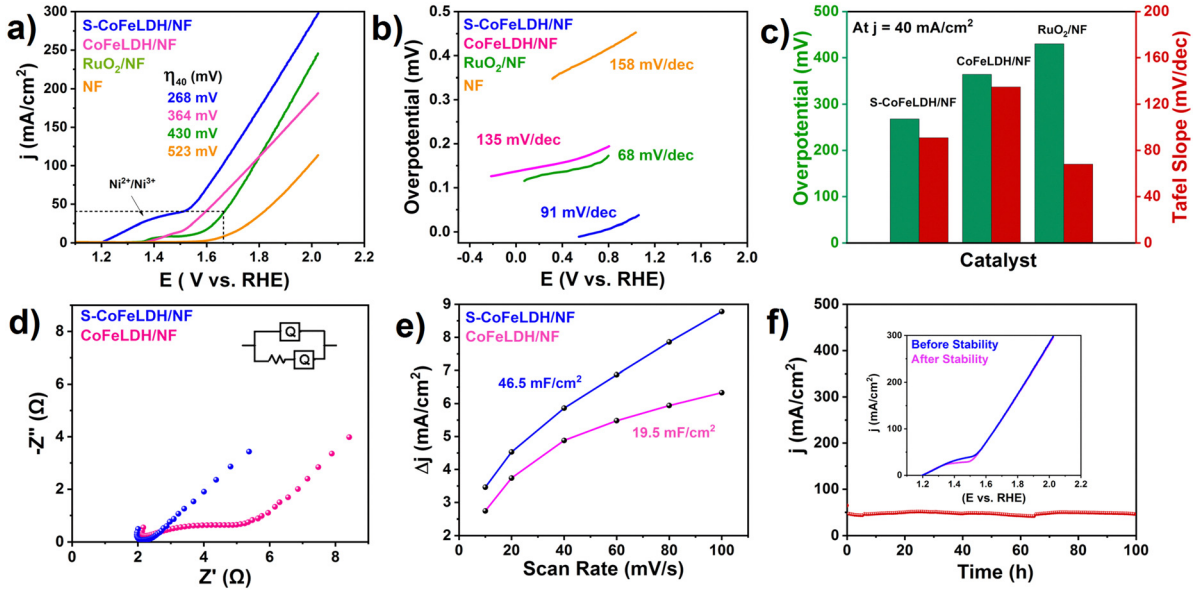

Fig. 3 Electrochemical characterization of S-CoFeLDH/NF for the OER in 1 M KOH. (a) LSV polarization curve of S-CoFeLDH with CoFeLDH and RuO_2. (b) Tafel slope. (c) Comparsion of catalysts in terms of overpotential and tafel slope. (d) EIS Nyquist plot with the inset representing the fitted circuit. (e) C_{dl} plot of S-CoFeLDH and CoFeLDH. (f) Long term chronoamperometric stability of 100 h with the inset showing before and after LSV curves.

the corresponding Tafel plots shown in Fig. 3(b). The relatively low Tafel slope value of S-CoFeLDH/NF (91 mV dec^{-1}) indicates a faster kinetics associated with the electrochemical activity as compared with other catalysts (68, 135 and 158 mV dec^{-1} for RuO_2/NF, CoFeLDH/NF and NF, respectively). The comparison of the S-CoFeLDH/NF electrocatalyst with supplementary catalysts in terms of the overpotential and Tafel slope is shown in Fig. 3(c), where S-CoFeLDH outperforms the pristine CoFeLDH and conventionally employed RuO_2. The internal charge transfer of the catalyst was interpreted using electrochemical impedance spectroscopy (EIS) as shown in Fig. 3(d).[37] Sulphur doped LDH has a lower R_{CT} value as compared to the pure LDH system. The R_{CT} value of S-CoFeLDH/NF was found to be 1.55 Ohm, whereas for CoFeLDH/NF, it is 3.10 Ohm indicating a faster charge transfer through the interface of the S-CoFeLDH/NF catalyst. The double layer capacitance of the catalyst (C_{dl}) was determined to be 46.5 mF cm^{-2} for S-CoFeLDH/NF and 19.5 mF cm^{-2} for CoFeLDH/NF (Fig. 3(e)). Several CV curves were plotted for S-CoFeLDH/NF and CoFeLDH/NF in the non-faradaic region to determine the C_{dl} value (ESI,† Fig. S4(a and b)). Based on the C_{dl} value, the electrochemically active surface area (ECSA) of S-CoFeLDH/NF is calculated (13.6 cm^2), which is about six times higher than that of CoFeLDH/NF, suggesting that sulphur incorporated CoFeLDH possesses more catalytic active sites for the OER than CoFeLDH (5.73 cm^2). Apart from the electrochemical properties, S-CoFeLDH/NF also exhibits a long term stability of 100 h in 1.0 M KOH, when measured at a current density of 50 mA cm^{-2} (Fig. 3(f)). The inset plot of Fig. 3(f) exhibits the LSV curve obtained before and after the stability experiment. The curves mostly show a fine overlap, suggesting a minimal change in electrochemical activity before and after stability. The apparent turnover frequency (TOF) of the corresponding reaction was also calculated for S-CoFeLDH/NF and was found to be 0.01 s^{-1} which was higher than that of pristine CoFeLDH (0.005 s^{-1}) (ESI,† Fig. S5). To assess the position of this catalyst among other LDH-based catalysts, a comparison database has been provided in Table S1 in the ESI.† This table compares the recently reported catalysts with S-CoFeLDH/NF for the oxygen evolution reaction (OER).

The UOR electrochemical performance was analysed in 1.0 M KOH and 0.5 M urea. As displayed in Fig. 4(a), S-CoFeLDH/NF required a lower overpotential for the UOR

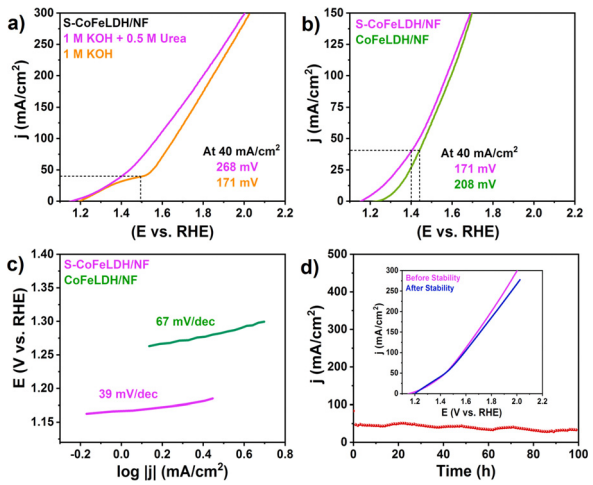

Fig. 4 Electrochemical characterization of S-CoFeLDH/NF for UOR in 1M KOH and 0.5 M urea. (a) LSV polarization curve (b) UOR polarization curve for S-CoFeLDH and CoFeLDH (c) Tafel slope (d) long term chronoamperometric stability of 120 h with inset showing before and after LSV curves.

(171 mV) as compared to the OER (268 mV), at a higher current density of 40 mA cm^{-2}. Fig. 4(b) shows the basic comparison of UOR catalytic activity of supplementary catalysts measured at 40 mA cm^{-2}. It was observed that S-CoFeLDH/NF and CoFeLDH/NF required an overpotential of 171 and 208 mV, respectively, for the UOR at a current density of 40 mA cm^{-2}. To investigate the kinetics of the UOR, Tafel slope calculation was performed (Fig. 4(c)) obtaining values of 39 and 67 mV dec^{-1} for S-CoFeLDH/NF and CoFeLDH/NF, respectively.

These values again indicate that incorporation of sulfur into LDHs results in the increase of UOR kinetics by 28 mV dec^{-1}. To determine the longevity of the catalyst, a long-term stability experiment was conducted at a current density of 50 mA cm^{-2} for 100 hours. The polarization curves depicted in the inset of Fig. 4(d) demonstrate that 98.5% of electrochemical activity was retained at 40 mA cm^{-2}. To analyse the electrochemical performance of S-CoFeLDH towards the UOR, the catalyst is compared with other currently reported LDH based catalysts, as displayed Table S2 in ESI.† S-CoFeLDH/NF also exhibits excellent C_{dl} with a capacitance value of 43.5 mF cm^{-2} as shown in Fig. S6(b) ESI.† The electrochemically active surface area (ECSA) was calculated for the UOR in comparison to S-CoFeLDH, and was found to be 12.79 cm^2. The electrochemical impedance curve (ESI,† Fig. S6(c)) shows a R_{CT} value of 0.56 Ohms, suggesting fast charge transfer along the electrolyte and electrode interface. A table comparing the bifunctional activities of the catalyst toward the OER and UOR, with respect to the previous relevant reports is shown in Table 1.[38–45]

After 100 h of prolonged OER stability experiment, the S-CoFeLDH/NF electrode was further characterized with FESEM and XPS. In FESEM images of S-CoFeLDH/NF (ESI,† Fig. S7) after the experiment, the morphology was retained and stood unaffected by an applied potential for a long time. The XPS analysis displays the decreased intensity of the M–S bond revealing the reconstruction of the S-based species to form surface metal hydroxysulfides thus affecting the surface electronic environment during the electrochemical reaction. After the prolonged stability experiment the continuous oxidation of the catalysts leads to the strengthening of the M–O bond that is observed in the high-resolution O 1s spectra. The metal ions remained unchanged without showing any shift in binding energies (ESI,† Fig. S8).

Additionally, to study the effect of competing anodic reactions for hydrogen generation, full cell measurements were performed for water and urea electrolysis. For overall water electrolysis two electrode setups were employed in 1 M KOH, whereas for overall urea electrolysis, the electrolyte used was 1 M KOH with 0.5 M urea. S-CoFeLDH||Pt/C was constructed as a full cell for water and urea electrolysis (Fig. 5(a)). For comparison, Pt/C and RuO_2 were used as benchmark catalysts for the HER and OER in the cell. The LSV results in Fig. 5(b) indicate that the cell requires a potential of 1.52 and 1.41 V for overall water and urea electrolysis at 10 mA cm^{-2}, respectively. To compare the results, RuO_2||Pt/C was employed as a full cell electrocatalyst and it exhibits a potential of 1.68 V to reach a current density of 10 mA cm^{-2}. Fig. 5(c) displaying the LSV curves on the smaller axis range, showing the corresponding potential at 10 mA cm^{-2}. The S-CoFeLDH||Pt/C cell outperforms the conventionally used catalytic cell RuO_2||Pt/C by 0.27 V and 0.16 V for urea and water electrolysis, respectively. Difference between the potential of overall water and urea electrolysis was ~0.11 V, which indicates that the urea oxidation at the anodic part can significantly increase the activity of an electrocatalyst, for hydrogen generation. The durability test of the catalyst for full cell reaction was performed at a higher current density of 50 mA cm^{-2}, using the chronoamperometric technique for 12 h. The catalyst was found to be stable in both water and urea electrolysis for more than 12 h. These results indicate that the methodology has significant potential for modifying existing electrode materials and can greatly enhance hydrogen generation.

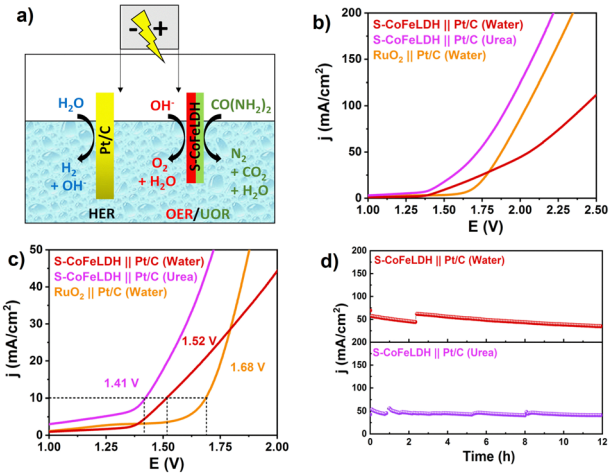

Fig. 5 Electrochemical characterization of S-CoFeLDH/NF for full cell electrolysis of water and urea. (a) Graphical illustration of the full cell. (b) LSV polarization curve for the full cell reaction with S-CoFeLDH||Pt/C in 1 M KOH with and without urea and RuO_2||Pt/C. (c) Zoomed LSV showing potential at 10 mA cm^{-2} and (d) chronoamperometric stability of 10 h for urea and water electrolysis.

Table 1 Comparison of onset potential of bifunctional electrocatalysts for the OER and UOR, at current densities of (a) 10 mA cm^{-2} and (b) 40 mA cm^{-2}

Year	Catalyst	$OER_{(E\ vs.\ RHE)}$ (V)	$UOR_{(E\ vs.\ RHE)}$ (V)
2023	S-CoFeLDH (this work)	1.49[b]	1.40[b]
2023	1.5 Mn-NiCo-HNS/CNT	1.47[a]	1.35[a]
2022	E-LDH/α-FeOOH	1.42[a]	1.37[a]
2022	Cu-Ni_3S_2@NiFeLDH	1.50[a]	1.41[a]
2021	CoO-Co_4N@NiFe-LDH	1.46[a]	1.39[a]
2021	CoFe LDH/MOF-0.06	1.50[a]	1.45[a]
2020	CoMnLDH	1.51[a]	1.32[a]
2019	NiFeCoLDH	1.44[a]	1.49[a]
2019	NiFeLDH-D	1.39[a]	1.32[a]

DFT calculations

DFT calculations were performed to understand the mechanism of the OER process with and without S-incorporation in CoFeLDH. The Gibbs free energy (ΔG) of the intermediates

formed during the OER (OH*, O*, OOH*) and adsorbed on the catalytic surface was calculated from the total energy of the supercell as discussed in the ESI.†[46] The computational details and formulae are given in the ESI.† Due to the partial sulfurization, the LDHs remained intact in the catalyst, which was confirmed by PXRD. Additionally, the XPS analyses revealed the replacement of few hydroxyl ions by sulfur on the catalytic surface. According to the experimental results, the hydroxyl groups present in the lattice above the surface were replaced by sulfur atoms in the lattice to perform DFT studies. The incorporation site for the S-atom was chosen by the fact that the surface hydroxyl ions were replaced by sulfur.[47] Also, the XPS results confirmed the existence of sulfur on the surface of the catalyst. Thus, S was added to the LDH substrate, by replacing a few hydroxyl groups and all the hydroxyl groups were not replaced because the LDH phase was intact in the catalyst even after the sulfurization. Additionally, the high resolution XPS suggests the formation of a M–S bond, thus sulfur was bonded with Co and Fe in the simulated structure. The adsorption energy of the catalyst and the adsorbed intermediates are shown in Table S3, ESI,† with the formulas used for calculating Gibbs free energy. Fig. 6(a) shows the LDH structure used for DFT calculations and Fig. 6(b) shows the OER mechanism with the simulated structure considering Co as the active site. Fig. 6(c) and (d) show the Gibbs free energy plot for Fe and Co active sites in S-CoFeLDH, respectively. It can be observed from the Gibbs free energy plot that the potential limiting step (PLS) for Fe and Co active sites has a value of 1.33 and 0.72 eV, respectively, suggesting Co to be the active site for the OER mechanism. In CoFeLDH, the three steps are uphill in both the cases (ESI,† Fig. S9), at 0 V and at an equilibrium potential of 1.23 V and the PLS has a value of 2.1 eV which is very high as compared to the Co active sites in S-CoFeLDH. In summary, the theoretical ΔG_{ads} values of CoFeLDH (Fe*), S-CoFeLDH/NF (Co*) and S-CoFeLDH/NF (Fe*) were 2.1 eV, 0.72 eV and 1.33 eV, respectively, suggesting Co as the preferred active site for the OER mechanism. These plots reveal that sulfurization lowers the Gibbs free energy for all intermediates allowing facile adsorption on electrocatalytic active areas as compared to pristine CoFeLDH. The feasibility of the OER is strongly dependent on the very frequent formation of the intermediates (M–OH*, M–O*, and M–OOH*) and facile adsorption and fast electron transfer which results in better electro-kinetics of the reaction. According to the reported mechanism for the UOR,[48] the reaction consists of six-steps, where the first step is the adsorption of urea, followed by dehydrogenation of N–H ($4e^-$) in the second step, in third step N_2 dissociates leaving CO adsorbed over the substrate followed by the formation of O═C–OH in the fourth step, further in an alkaline medium O═C–OH transforms into CO_3^{2-} in the fifth step, followed by the release of CO_2 shown in Fig. S10 in the ESI.†[49] The projected density of states (PDOS) are plotted in Fig. 6(e) and (f), where both the catalysts show metallic behavior. The increased p–d mixing in the catalyst will give rise to hybridized orbitals for a stable catalytic substrate owing to the homogeneous charge distribution over the surface. Also, the electron transmission capacity is enhanced between the overlapped mixed orbitals of sulfurized LDH, which leads to enhancement of the electrochemical activity of S-CoFeLDH.[50] The total density of states (TDOS) calculation was performed to verify the overall effect of sulfurization over the electronic structure shown in Fig. S11, ESI.†. The TDOS results indicated that the area under the curve was substantially increased after sulfurization, suggesting the enhanced density of states which leads to boost the electrochemical activity of S-CoFeLDH. Furthermore, the enhanced DOS near the Fermi surface indicates the higher carrier density and conductivity that facilitate electron transfer during the UOR.[51] Additionally, the differential charge density was calculated as shown in Fig. S12, ESI.† The increased charge accumulation (blue) and depletion (yellow) was observed over the

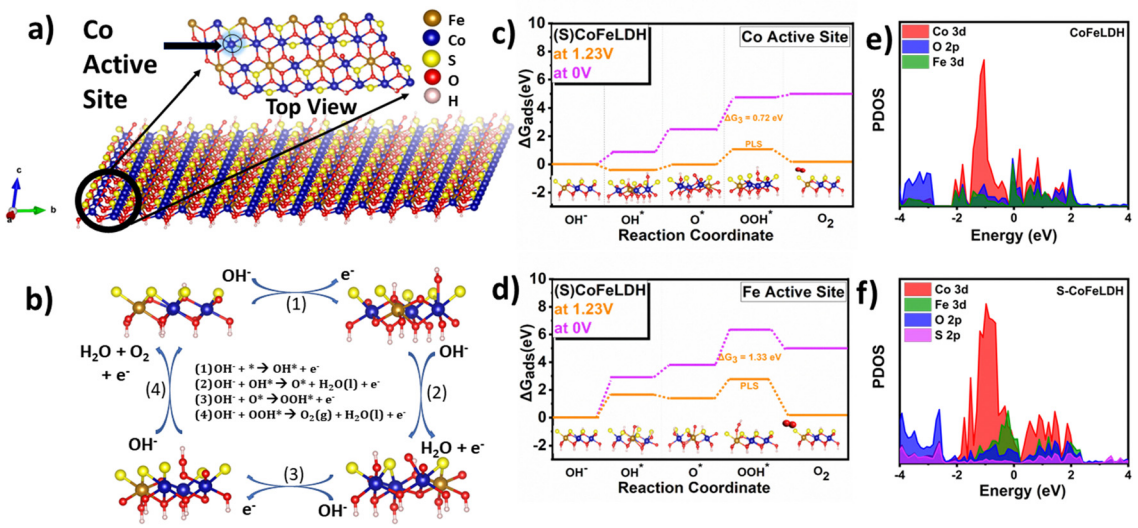

Fig. 6 (a) Theoretically simulated active site illustration. (b) OER mechanism. (c) and (d) Gibbs free energy plot of S-CoFeLDH on Co and Fe active sites, respectively. (e) and (f) PDOS plot of CoFeLDH and S-CoFeLDH.

catalytic surface, and was responsible for the enhanced electrochemical activity towards anodic reactions after sulfurization.

Conclusion

In summary, we have reported a simple two-step practical approach to introduce sulfur over cobalt iron LDH nanosheets for OER/UOR applications. A 3D-flower like architecture was made out of packed nanosheets of S-CoFeLDH, grown on nickel foam (NF). The incorporation of heteroatoms into the existing LDH system significantly enhanced the charge transfer capability, increased the exposure of active sites, and lowered the potential barrier for anodic reactions. This resulted in decreased overpotentials of 268 mV and 171 mV for the OER and UOR at a current density of 40 mA cm^{-2}, respectively. A long-term activity test for the catalyst was conducted for over 100 hours for both the OER and UOR. The results showed that the catalyst is highly stable throughout the reaction process. The DFT results suggest that "Co" is a more prominent active site for the oxygen evolution reaction (OER) in S-CoFeLDH compared to Co-FeLDH. The p–d mixing between the metal d orbital and p orbital of S and O is responsible for the enhanced electron transfer process which further augments the electrochemical activity of S-CoFeLDH/NF towards OER/UOR. X-Ray photoelectron spectroscopy measurements have also revealed the oxidation states of Co^{2+}, Fe^{3+} and S^{2-}, indicating them to be flexible hosts to adsorb intermediates. S-CoFeLDH/NF has shown good electrochemical activity towards the OER and UOR. For future perspective, this analogy can be followed to exploit other LDH based materials which left unexplored for anodic reactions like the OER and UOR. This study also explores the potential to utilize derivatives of LDHs in order to overcome the high overpotential of the OER in the process of hydrogen generation. These LDH derivatives may offer a superior alternative (UOR) to traditional anodic reactions and provide an opportunity to improve the efficiency of hydrogen production.

Author contributions

This manuscript was written through contributions of all authors.

Conflicts of interest

There are no conflicts to declare.

Acknowledgements

VB appreciates the financial support from the Department of Science and Technology (DST, CRG/2022/006402). KK acknowledges INST for PhD fellowship.

References

1 Joint Research Centre (European Commission); J. G. J. Olivier, D. Guizzardi, E. Schaaf, E. Solazzo, M. Crippa, E. Vignati, M. Banja, M. Muntean, G. Grassi, F. Monforti-Ferrario and S. Rossi, GHG Emissions of All World: 2021 Report, Publications Office of the European Union: LU, 2021.

2 Z. Dai, X. Du and X. Zhang, Controlled Synthesis of NiCo2O4@Ni-MOF on Ni Foam as Efficient Electrocatalyst for Urea Oxidation Reaction and Oxygen Evolution Reaction, *Int. J. Hydrogen Energy*, 2022, **47**(39), 17252–17262, DOI: **10.1016/j.ijhydene.2022.03.217**.

3 S. A. Patil, N. K. Shrestha, H. T. Bui, V. D. Chavan, D. Kim, S. F. Shaikh, M. Ubaidullah, H. Kim and H. Im, Solvent Modulated Self-Assembled VS2 Layered Microstructure for Electrocatalytic Water and Urea Decomposition, *Int. J. Energy Res.*, 2022, **46**(6), 8413–8423, DOI: **10.1002/er.7651**.

4 S. A. Patil, S. Cho, Y. Jo, N. K. Shrestha, H. Kim and H. Im, Bimetallic Ni-Co@hexacyano Nano-Frameworks Anchored on Carbon Nanotubes for Highly Efficient Overall Water Splitting and Urea Decontamination, *Chem. Eng. J.*, 2021, **426**, 130773, DOI: **10.1016/j.cej.2021.130773**.

5 Z. Dai, X. Du, Y. Wang, X. Han and X. Zhang, Promoting Urea Oxidation and Water Oxidation through Interface Construction on a CeO2@CoFe2O4 Heterostructure, *Dalton Trans.*, 2021, **50**(35), 12301–12307, DOI: **10.1039/D1DT01952J**.

6 X. Sun and R. Ding, Recent Progress with Electrocatalysts for Urea Electrolysis in Alkaline Media for Energy-Saving Hydrogen Production, *Catal. Sci. Technol.*, 2020, **10**(6), 1567–1581, DOI: **10.1039/C9CY02618E**.

7 Z.-Y. Yu, C.-C. Lang, M.-R. Gao, Y. Chen, Q.-Q. Fu, Y. Duan and S.-H. Yu, Ni–Mo–O Nanorod-Derived Composite Catalysts for Efficient Alkaline Water-to-Hydrogen Conversion via Urea Electrolysis, *Energy Environ. Sci.*, 2018, **11**(7), 1890–1897, DOI: **10.1039/C8EE00521D**.

8 Q. Wang, X. Cheng, Y. Sun, Z. Sun, D. Wang, G. Chen and P. Schaaf, A Synergetic Effect between Photogenerated Carriers and Photothermally Enhanced Electrochemical Urea-Assisted Hydrogen Generation on the Ni-NiO/Nickel Foam Catalyst, *Mater. Adv.*, 2021, **2**(6), 2104–2111, DOI: **10.1039/D1MA00038A**.

9 X. Hu, J. Zhu, J. Li and Q. Wu, Urea Electrooxidation: Current Development and Understanding of Ni-Based Catalysts, *ChemElectroChem*, 2020, **7**(15), 3211–3228, DOI: **10.1002/celc.202000404**.

10 K. Cho and M. R. Hoffmann, Urea Degradation by Electrochemically Generated Reactive Chlorine Species: Products and Reaction Pathways, *Environ. Sci. Technol.*, 2014, **48**(19), 11504–11511, DOI: **10.1021/es5025405**.

11 J. Ge, Y. Lai, M. Guan, Y. Xiao, J. Kuang and C. Yang, Nickel Borate with a 3D Hierarchical Structure as a Robust and Efficient Electrocatalyst for Urea Oxidation, *Environ. Sci.: Nano*, 2021, **8**(5), 1326–1335, DOI: **10.1039/D0EN01247E**.

12 B. K. Boggs, R. L. King and G. G. Botte, Urea Electrolysis: Direct Hydrogen Production from Urine, *Chem. Commun.*, 2009, (32), 4859–4861, DOI: **10.1039/B905974A**.

13 Md. S. Islam, M. Kim, X. Jin, S. M. Oh, N.-S. Lee, H. Kim and S.-J. Hwang, Bifunctional 2D Superlattice Electrocatalysts of Layered Double Hydroxide–Transition Metal Dichalcogenide

Active for Overall Water Splitting, *ACS Energy Lett.*, 2018, **3**(4), 952–960, DOI: 10.1021/acsenergylett.8b00134.

14 M. Krishankant, M. Aashi, Z. Ahmed, S. Alagar, A. Gaur, R. Kaur and V. Bagchi, Nano-Interfaced Tungsten Oxide Decorated on Layered Double Hydroxides for the Oxygen Evolution Reaction, *Sustainable Energy Fuels*, 2022, **6**, 4429–4436, DOI: 10.1039/D2SE00929C.

15 L. Chen, Y. Guo, H. Wang, Z. Gu, Y. Zhang, X. Li, H. Wang and C. Duan, Imidazolate-Mediated Assembled Structures of Co-LDH Sheets for Efficient Electrocatalytic Oxygen Evolution, *J. Mater. Chem. A*, 2018, **6**(11), 4636–4641, DOI: 10.1039/C7TA11078B.

16 S. J. Patil, N. R. Chodankar, S.-K. Hwang, G. S. Rama Raju, Y.-S. Huh and Y.-K. Han, Fluorine Engineered Self-Supported Ultrathin 2D Nickel Hydroxide Nanosheets as Highly Robust and Stable Bifunctional Electrocatalysts for Oxygen Evolution and Urea Oxidation Reactions, *Small*, 2022, **18**(7), 2103326, DOI: 10.1002/smll.202103326.

17 M. Wang, L. Zhang, Y. He and H. Zhu, Recent Advances in Transition-Metal-Sulfide-Based Bifunctional Electrocatalysts for Overall Water Splitting, *J. Mater. Chem. A*, 2021, **9**(9), 5320–5363, DOI: 10.1039/D0TA12152E.

18 C. (Rose) Zhu, D. Gao, J. Ding, D. Chao and J. Wang, TMD-Based Highly Efficient Electrocatalysts Developed by Combined Computational and Experimental Approaches, *Chem. Soc. Rev.*, 2018, **47**(12), 4332–4356, DOI: 10.1039/C7CS00705A.

19 R. Subbaraman, D. Tripkovic, K.-C. Chang, D. Strmcnik, A. P. Paulikas, P. Hirunsit, M. Chan, J. Greeley, V. Stamenkovic and N. M. Markovic, Trends in Activity for the Water Electrolyser Reactions on 3d M(Ni,Co,Fe,Mn) Hydr(Oxy)Oxide Catalysts, *Nat. Mater.*, 2012, **11**(6), 550–557, DOI: 10.1038/nmat3313.

20 J. Joo, T. Kim, J. Lee, S.-I. Choi and K. Lee, Morphology-Controlled Metal Sulfides and Phosphides for Electrochemical Water Splitting, *Adv. Mater.*, 2019, **31**(14), 1806682, DOI: 10.1002/adma.201806682.

21 M. Cai, Q. Zhu, X. Wang, Z. Shao, L. Yao, H. Zeng, X. Wu, J. Chen, K. Huang and S. Feng, Formation and Stabilization of NiOOH by Introducing α-FeOOH in LDH: Composite Electrocatalyst for Oxygen Evolution and Urea Oxidation Reactions, *Adv. Mater.*, 2022, 2209338, DOI: 10.1002/adma.202209338.

22 H. Sun, Z. Yan, F. Liu, W. Xu, F. Cheng and J. Chen, Self-Supported Transition-Metal-Based Electrocatalysts for Hydrogen and Oxygen Evolution, *Adv. Mater.*, 2020, **32**(3), 1806326, DOI: 10.1002/adma.201806326.

23 C. Du, M. Shang, J. Mao and W. Song, Hierarchical MoP/Ni_2P Heterostructures on Nickel Foam for Efficient Water Splitting, *J. Mater. Chem. A*, 2017, **5**(30), 15940–15949, DOI: 10.1039/C7TA03669H.

24 K. Nguyen, N. D. Hoa, C. M. Hung, D. T. T. Le, N. V. Duy and N. V. Hieu, A Comparative Study on the Electrochemical Properties of Nanoporous Nickel Oxide Nanowires and Nanosheets Prepared by a Hydrothermal Method, *RSC Adv.*, 2018, **8**(35), 19449–19455, DOI: 10.1039/C8RA02862A.

25 J. Paier, R. Hirschl, M. Marsman and G. Kresse, The Perdew–Burke–Ernzerhof Exchange-Correlation Functional Applied to the G2-1 Test Set Using a Plane-Wave Basis Set, *J. Chem. Phys.*, 2005, **122**(23), 234102, DOI: 10.1063/1.1926272.

26 A. Sivanantham, P. Ganesan and S. Shanmugam, Hierarchical NiCo2S4 Nanowire Arrays Supported on Ni Foam: An Efficient and Durable Bifunctional Electrocatalyst for Oxygen and Hydrogen Evolution Reactions, *Adv. Funct. Mater.*, 2016, **26**(26), 4661–4672, DOI: 10.1002/adfm.201600566.

27 M. Al-Mamun, Z. Zhu, H. Yin, X. Su, H. Zhang, P. Liu, H. Yang, D. Wang, Z. Tang, Y. Wang and H. Zhao, The Surface Sulfur Doping Induced Enhanced Performance of Cobalt Catalysts in Oxygen Evolution Reactions, *Chem. Commun.*, 2016, **52**(60), 9450–9453, DOI: 10.1039/C6CC04387A.

28 Z. Wan, Z. Ma, H. Yuan, K. Liu and X. Wang, Sulfur Engineering on NiFe Layered Double Hydroxide at Ambient Temperature for High Current Density Oxygen Evolution Reaction, *ACS Appl. Energy Mater.*, 2022, **5**(4), 4603–4612, DOI: 10.1021/acsaem.2c00018.

29 L.-L. Liu, D.-H. Wu, L. Zhang, J.-J. Feng and A.-J. Wang, FeCo Alloy Entrapped in N-Doped Graphitic Carbon Nanotubes-on-Nanosheets Prepared by Coordination-Induced Pyrolysis for Oxygen Reduction Reaction and Rechargeable Zn-Air Battery, *J. Colloid Interface Sci.*, 2023, **639**, 424–433, DOI: 10.1016/j.jcis.2023.02.061.

30 Y. Li and C. Zhao, Enhancing Water Oxidation Catalysis on a Synergistic Phosphorylated NiFe Hydroxide by Adjusting Catalyst Wettability, *ACS Catal.*, 2017, **7**(4), 2535–2541, DOI: 10.1021/acscatal.6b03497.

31 D.-H. Wu, H. Huang, M. Ul Haq, L. Zhang, J.-J. Feng and A.-J. Wang, Lignin-Derived Iron Carbide/Mn, N, S-Codoped Carbon Nanotubes as a High-Efficiency Catalyst for Synergistically Enhanced Oxygen Reduction Reaction and Rechargeable Zinc-Air Battery, *J. Colloid Interface Sci.*, 2023, **647**, 1–11, DOI: 10.1016/j.jcis.2023.05.111.

32 C. Zhang, Y. Huang, Y. Yu, J. Zhang, S. Zhuo and B. Zhang, Sub-1.1 Nm Ultrathin Porous CoP Nanosheets with Dominant Reactive {200} Facets: A High Mass Activity and Efficient Electrocatalyst for the Hydrogen Evolution Reaction, *Chem. Sci.*, 2017, **8**(4), 2769–2775, DOI: 10.1039/C6SC05687C.

33 W. Xu, J. Chen, M. Yu, Y. Zeng, Y. Long, X. Lu and Y. Tong, Sulphur-Doped Co_3O_4 Nanowires as an Advanced Negative Electrode for High-Energy Asymmetric Supercapacitors, *J. Mater. Chem. A*, 2016, **4**(28), 10779–10785, DOI: 10.1039/C6TA03153F.

34 B.-Q. Li, S.-Y. Zhang, C. Tang, X. Cui and Q. Zhang, Anionic Regulated NiFe (Oxy)Sulfide Electrocatalysts for Water Oxidation, *Small*, 2017, **13**(25), 1700610, DOI: 10.1002/smll.201700610.

35 L. Zhang, Y.-T. Ma, J.-J. Duan, Y.-Q. Yao, J.-J. Feng and A.-J. Wang, *In Situ* Construction of 3D Hetero-Structured Sulfur-Doped Nanoflower-like FeNi LDH Decorated with NiCo Prussian Blue Analogue Cubes as Efficient Electrocatalysts for Boosting Oxygen Evolution Reaction, *J. Colloid Interface Sci.*, 2022, **611**, 205–214, DOI: 10.1016/j.jcis.2021.12.066.

36 C.-X. Zhao, B.-Q. Li, M. Zhao, J.-N. Liu, L.-D. Zhao, X. Chen and Q. Zhang, Precise Anionic Regulation of NiFe

Hydroxysulfide Assisted by Electrochemical Reactions for Efficient Electrocatalysis, *Energy Environ. Sci.*, 2020, **13**(6), 1711–1716, DOI: **10.1039/C9EE03573G**.

37 C. Xia, Q. Jiang, C. Zhao, M. N. Hedhili and H. N. Alshareef, Selenide-Based Electrocatalysts and Scaffolds for Water Oxidation Applications, *Adv. Mater.*, 2016, **28**(1), 77–85, DOI: **10.1002/adma.201503906**.

38 C. Zhang, T. Chen, H. Zhang, Z. Li and J. Hao, Hydrated-Metal-Halide-Based Deep-Eutectic-Solvent-Mediated NiFe Layered Double Hydroxide: An Excellent Electrocatalyst for Urea Electrolysis and Water Splitting, *Chem. – Asian J.*, 2019, **14**(17), 2995–3002, DOI: **10.1002/asia.201900742**.

39 M. Cai, Q. Zhu, X. Wang, Z. Shao, L. Yao, H. Zeng, X. Wu, J. Chen, K. Huang and S. Feng, Formation and Stabilization of NiOOH by Introducing α-FeOOH in LDH: Composite Electrocatalyst for Oxygen Evolution and Urea Oxidation Reactions, *Adv. Mater.*, 2022, 2209338, DOI: **10.1002/adma.202209338**.

40 P. Babar, A. Lokhande, V. Karade, B. Pawar, M. G. Gang, S. Pawar and J. H. Kim, Bifunctional 2D Electrocatalysts of Transition Metal Hydroxide Nanosheet Arrays for Water Splitting and Urea Electrolysis, *ACS Sustainable Chem. Eng.*, 2019, **7**(11), 10035–10043, DOI: **10.1021/acssuschemeng.9b01260**.

41 B. Chen, M. Humayun, Y. Li, H. Zhang, H. Sun, Y. Wu and C. Wang, Constructing Hierarchical Fluffy CoO–Co $_4$ N@NiFe-LDH Nanorod Arrays for Highly Effective Overall Water Splitting and Urea Electrolysis, *ACS Sustainable Chem. Eng.*, 2021, **9**(42), 14180–14192, DOI: **10.1021/acssuschemeng.1c04674**.

42 K. Wu, C. Cao, K. Li, C. Lyu, J. Cheng, H. Li, P. Hu, J. Wu, W.-M. Lau, X. Zhu, P. Qian and J. Zheng, Regulating Electronic Structure by Mn Doping for Nickel Cobalt Hydroxide Nanosheets/Carbon Nanotube to Promote Oxygen Evolution Reaction and Oxidation of Urea and Hydrazine, *Chem. Eng. J.*, 2023, **452**, 139527, DOI: **10.1016/j.cej.2022.139527**.

43 Y. Ding, X. Du and X. Zhang, Rose-like Cu-Doped Ni3S2 Nanoflowers Decorated with Thin NiFe LDH Nanosheets for High-Efficiency Overall Water and Urea Electrolysis, *Appl. Surf. Sci.*, 2022, **584**, 152622, DOI: **10.1016/j.apsusc.2022.152622**.

44 S. Huang, Y. Wu, J. Fu, P. Xin, Q. Zhang, Z. Jin, J. Zhang, Z. Hu and Z. Chen, Hierarchical CoFe LDH/MOF Nanorods Array with Strong Coupling Effect Grown on Carbon Cloth Enables Efficient Oxidation of Water and Urea, *Nanotechnology*, 2021, **32**(38), 385405, DOI: **10.1088/1361-6528/ac0b65**.

45 Z. Wang, Y. Hu, W. Liu, L. Xu, M. Guan, Y. Zhao, J. Bao and H. Li, Manganese-Modulated Cobalt-Based Layered Double Hydroxide Grown on Nickel Foam with 1D–2D–3D Heterostructure for Highly Efficient Oxygen Evolution Reaction and Urea Oxidation Reaction, *Chem. – Eur. J.*, 2020, **26**(42), 9382–9388, DOI: **10.1002/chem.202001055**.

46 I. C. Man, H.-Y. Su, F. Calle-Vallejo, H. A. Hansen, J. I. Martínez, N. G. Inoglu, J. Kitchin, T. F. Jaramillo, J. K. Nørskov and J. Rossmeisl, Universality in Oxygen Evolution Electrocatalysis on Oxide Surfaces, *ChemCatChem*, 2011, **3**(7), 1159–1165, DOI: **10.1002/cctc.201000397**.

47 A. Sivanantham, P. Ganesan and S. Shanmugam, Hierarchical NiCo2S4 Nanowire Arrays Supported on Ni Foam: An Efficient and Durable Bifunctional Electrocatalyst for Oxygen and Hydrogen Evolution Reactions, *Adv. Funct. Mater.*, 2016, **26**(26), 4661–4672, DOI: **10.1002/adfm.201600566**.

48 Z. Ji, Y. Song, S. Zhao, Y. Li, J. Liu and W. Hu, Pathway Manipulation via Ni, Co, and V Ternary Synergism to Realize High Efficiency for Urea Electrocatalytic Oxidation, *ACS Catal.*, 2022, **12**(1), 569–579, DOI: **10.1021/acscatal.1c05190**.

49 Z. Wei, W. Sun, S. Liu, J. Qi, L. Kang, J. Li, S. Lou, J. Xie, B. Tang and Y. Xie, Lanthanum-Doped α-Ni(OH)2 1D-2D-3D Hierarchical Nanostructures for Robust Bifunctional Electro-Oxidation, *Particuology*, 2021, **57**, 104–111, DOI: **10.1016/j.partic.2021.01.002**.

50 H. Yang, M. Yuan, Z. Sun, D. Wang, L. Lin, H. Li and G. Sun, In Situ Construction of a Mn2 + -Doped Ni3S2 Electrode with Highly Enhanced Urea Oxidation Reaction Performance. *ACS Sustainable*, *Chem. Eng.*, 2020, **8**(22), 8348–8355, DOI: **10.1021/acssuschemeng.0c02160**.

51 Y. Tong, P. Chen, M. Zhang, T. Zhou, L. Zhang, W. Chu, C. Wu and Y. Xie, Oxygen Vacancies Confined in Nickel Molybdenum Oxide Porous Nanosheets for Promoted Electrocatalytic Urea Oxidation, *ACS Catal.*, 2018, **8**(1), 1–7, DOI: **10.1021/acscatal.7b03177**.